A search for flavor-changing non-standard neutrino interactions using ν_e appearance in MINOS

P. Adamson,[7] I. Anghel,[14,1] A. Aurisano,[6] G. Barr,[20] M. Bishai,[2] A. Blake,[4,*] G. J. Bock,[7] D. Bogert,[7] S. V. Cao,[28] T. J. Carroll,[28] C. M. Castromonte,[8] R. Chen,[16] S. Childress,[7] J. A. B. Coelho,[29] L. Corwin,[13,†] D. Cronin-Hennessy,[17] J. K. de Jong,[20] S. De Rijck,[28] A. V. Devan,[31] N. E. Devenish,[26] M. V. Diwan,[2] C. O. Escobar,[5] J. J. Evans,[16] E. Falk,[26] G. J. Feldman,[9] W. Flanagan,[28] M. V. Frohne,[10,‡] M. Gabrielyan,[17] H. R. Gallagher,[29] S. Germani,[15] R. A. Gomes,[8] M. C. Goodman,[1] P. Gouffon,[23] N. Graf,[12,21] R. Gran,[18] K. Grzelak,[30] A. Habig,[18] S. R. Hahn,[7] J. Hartnell,[26] R. Hatcher,[7] A. Holin,[15] J. Huang,[28] J. Hylen,[7] G. M. Irwin,[25] Z. Isvan,[2,21] C. James,[7] D. Jensen,[7] T. Kafka,[29] S. M. S. Kasahara,[17] G. Koizumi,[7] M. Kordosky,[31] A. Kreymer,[7] K. Lang,[28] J. Ling,[2] P. J. Litchfield,[17,22] P. Lucas,[7] W. A. Mann,[29] M. L. Marshak,[17] N. Mayer,[29,13] C. McGivern,[21] M. M. Medeiros,[8] R. Mehdiyev,[28] J. R. Meier,[17] M. D. Messier,[13] W. H. Miller,[17] S. R. Mishra,[24] S. Moed Sher,[7] C. D. Moore,[7] L. Mualem,[3] J. Musser,[13] D. Naples,[21] J. K. Nelson,[31] H. B. Newman,[3] R. J. Nichol,[15] J. A. Nowak,[17,*] J. O'Connor,[15] M. Orchanian,[3] R. B. Pahlka,[7] J. Paley,[1] R. B. Patterson,[3] G. Pawloski,[17,25] A. Perch,[15] M. M. Pfützner,[15] D. D. Phan,[28] S. Phan-Budd,[1] R. K. Plunkett,[7] N. Poonthottathil,[7] X. Qiu,[25] A. Radovic,[31] B. Rebel,[7] C. Rosenfeld,[24] H. A. Rubin,[12] P. Sail,[28] M. C. Sanchez,[14,1] J. Schneps,[29] A. Schreckenberger,[28,17] P. Schreiner,[1] R. Sharma,[7] A. Sousa,[6,9] N. Tagg,[19] R. L. Talaga,[1] J. Thomas,[15] M. A. Thomson,[4] X. Tian,[24] A. Timmons,[16] J. Todd,[6] S. C. Tognini,[8] R. Toner,[9,4] D. Torretta,[7] G. Tzanakos,[32,‡] J. Urheim,[13] P. Vahle,[31] B. Viren,[2] A. Weber,[20,22] R. C. Webb,[27] C. White,[12] L. Whitehead,[11,2] L. H. Whitehead,[15] S. G. Wojcicki,[25] and R. Zwaska[7]

(The MINOS Collaboration)

[1] *Argonne National Laboratory, Argonne, Illinois 60439, USA*
[2] *Brookhaven National Laboratory, Upton, New York 11973, USA*
[3] *Lauritsen Laboratory, California Institute of Technology, Pasadena, California 91125, USA*
[4] *Cavendish Laboratory, University of Cambridge, Madingley Road, Cambridge CB3 0HE, United Kingdom*
[5] *Universidade Estadual de Campinas, IFGW-UNICAMP, CP 6165, 13083-970, Campinas, SP, Brazil*
[6] *Department of Physics, University of Cincinnati, Cincinnati, Ohio 45221, USA*
[7] *Fermi National Accelerator Laboratory, Batavia, Illinois 60510, USA*
[8] *Instituto de Física, Universidade Federal de Goiás, 74690-900, Goiânia, GO, Brazil*
[9] *Department of Physics, Harvard University, Cambridge, Massachusetts 02138, USA*
[10] *Holy Cross College, Notre Dame, Indiana 46556, USA*
[11] *Department of Physics, University of Houston, Houston, Texas 77204, USA*
[12] *Department of Physics, Illinois Institute of Technology, Chicago, Illinois 60616, USA*
[13] *Indiana University, Bloomington, Indiana 47405, USA*
[14] *Department of Physics and Astronomy, Iowa State University, Ames, Iowa 50011 USA*
[15] *Department of Physics and Astronomy, University College London, Gower Street, London WC1E 6BT, United Kingdom*
[16] *School of Physics and Astronomy, University of Manchester, Oxford Road, Manchester M13 9PL, United Kingdom*
[17] *University of Minnesota, Minneapolis, Minnesota 55455, USA*
[18] *Department of Physics, University of Minnesota Duluth, Duluth, Minnesota 55812, USA*
[19] *Otterbein College, Westerville, Ohio 43081, USA*
[20] *Subdepartment of Particle Physics, University of Oxford, Oxford OX1 3RH, United Kingdom*
[21] *Department of Physics and Astronomy, University of Pittsburgh, Pittsburgh, Pennsylvania 15260, USA*
[22] *Rutherford Appleton Laboratory, Science and Technology Facilities Council, Didcot, OX11 0QX, United Kingdom*
[23] *Instituto de Física, Universidade de São Paulo, CP 66318, 05315-970, São Paulo, SP, Brazil*
[24] *Department of Physics and Astronomy, University of South Carolina, Columbia, South Carolina 29208, USA*
[25] *Department of Physics, Stanford University, Stanford, California 94305, USA*
[26] *Department of Physics and Astronomy, University of Sussex, Falmer, Brighton BN1 9QH, United Kingdom*
[27] *Physics Department, Texas A&M University, College Station, Texas 77843, USA*
[28] *Department of Physics, University of Texas at Austin, 1 University Station C1600, Austin, Texas 78712, USA*
[29] *Physics Department, Tufts University, Medford, Massachusetts 02155, USA*
[30] *Department of Physics, University of Warsaw, Pasteura 5, PL-02-093 Warsaw, Poland*
[31] *Department of Physics, College of William & Mary, Williamsburg, Virginia 23187, USA*
[32] *Department of Physics, University of Athens, GR-15771 Athens, Greece*

We report new constraints on flavor-changing non-standard neutrino interactions from the MINOS long-baseline experiment using ν_e appearance candidate events from a predominantly ν_μ beam. We

used a statistical selection algorithm to separate ν_e candidates from background events, enabling an analysis of the combined MINOS neutrino and antineutrino data. We observe no deviations from standard neutrino mixing, and thus place constraints on the non-standard interaction matter effect, $\varepsilon_{e\tau}$, and phase, $(\delta_{CP} + \delta_{e\tau})$, using a thirty-bin likelihood fit.

PACS numbers: 14.60.Pq, 14.60.Lm, 13.15.+g, 29.27.-a

Results from solar, atmospheric, reactor and accelerator experiments [1–7] demonstrate that neutrinos undergo flavor change as they propagate. This phenomenon is well described by a quantum mechanical mixing of the neutrino flavors. In the standard three-flavor oscillation model, this process can be parameterized by three angles, θ_{12}, θ_{13}, θ_{23}, and a CP-violating phase, δ_{CP} [8]. Electron neutrinos and antineutrinos propagating through matter are subjected to the Mikheyev-Smirnov-Wolfenstein (MSW) effect [9], which arises from forward coherent scattering with electrons in media. While this process itself does not change lepton flavor, the scattering modifies the probabilities for neutrinos to oscillate between flavor states.

Non-standard interactions (NSI) [10, 11] that enter the oscillation model permit additional interactions between matter and all neutrino flavors. Analogous to the MSW Hamiltonian, NSI effects can be written as a perturbation to the Hamiltonian associated with standard neutrino oscillation,

$$H_{NSI} = \sqrt{2} G_F N_e \begin{bmatrix} 1+\varepsilon_{ee} & \varepsilon_{e\mu} & \varepsilon_{e\tau} \\ \varepsilon^*_{e\mu} & \varepsilon_{\mu\mu} & \varepsilon_{\mu\tau} \\ \varepsilon^*_{e\tau} & \varepsilon^*_{\mu\tau} & \varepsilon_{\tau\tau} \end{bmatrix}. \qquad (1)$$

This addition depends upon the matter potential $V = \sqrt{2} G_F N_e$, where G_F is the Fermi coupling constant and N_e is the electron density of the traversed material; as well as the $\varepsilon_{\alpha\beta}$ coefficients, which indicate the strength of the NSI couplings.

The net impact of adding NSI to the standard three-flavor neutrino oscillation model yields nine additional free parameters: the six $\varepsilon_{\alpha\beta}$ terms and three additional CP-violating phases, $\delta_{e\tau}$, $\delta_{e\mu}$, and $\delta_{\mu\tau}$.

Searches for NSI have already been performed on an atmospheric neutrino sample at Super-Kamiokande [12], the ν_μ and $\overline{\nu}_\mu$ survival channels at MINOS [13–16], and ν_e and $\overline{\nu}_e$ appearance channels in MINOS and T2K [17]. Long-baseline accelerator-based experiments offer well-defined propagation lengths and tunable energy spectra that benefit oscillation searches, including investigations of potential NSI phenomena.

MINOS [18] uses two magnetized steel-scintillator tracking calorimeters placed along the NuMI beamline [19] to study neutrino oscillation. In the NuMI beam, pions and kaons are produced from interactions between incident 120 GeV protons and a graphite target. Charged particles are subsequently focused by a pair of current-pulsed aluminum horns, and the decays of these particles in a 675 m decay pipe yield neutrinos. Remaining hadrons are captured by an absorber at the end of the decay pipe, and muons are removed from the beam by 240 meters of rock that separate the absorber from the detector hall. The neutrino energy spectrum depends upon the configuration of the focusing horns. For this analysis, the reconstructed energy spectrum peaked at around 3 GeV.

The 0.98 kiloton Near Detector (ND) is located 1.04 km downstream of the NuMI target at the Fermi National Accelerator Laboratory. It provides observations of the initial composition of the neutrino beam. From Monte Carlo simulations at the ND, we determined that the beam consists of 91.7% ν_μ, 7.0% $\overline{\nu}_\mu$, and 1.3% $(\nu_e + \overline{\nu}_e)$ when operated in neutrino mode, and 58.1% ν_μ, 39.9% $\overline{\nu}_\mu$, and 2.0% $(\nu_e + \overline{\nu}_e)$ when operated in antineutrino mode [20]. The 5.4 kiloton Far Detector (FD), situated in the Soudan Mine in northeastern Minnesota 735 km downstream of the NuMI target, registers neutrino interactions and permits searches for oscillation phenomena.

MINOS has investigated the ν_e appearance channel, yielding constraints on both the θ_{13} and δ_{CP} mixing parameters [20, 22]. The tightest constraints on θ_{13} come from reactor neutrino experiments, which have shown the parameter to be non-zero [7]. By using the MINOS ν_e and $\overline{\nu}_e$ appearance data in conjunction with these reactor results, limits can be placed upon the $\varepsilon_{e\tau}$ parameter. This technique is demonstrated in [17], which obtained confidence limits on $\varepsilon_{e\tau}$ based upon the MINOS and T2K ν_e appearance event rates. In this paper, we expand upon the analysis of $\varepsilon_{e\tau}$ by utilizing the observed energy spectra of ν_e and $\overline{\nu}_e$ appearance candidates along with a full treatment of the systematic uncertainties. We adopt the same techniques and MINOS exposure as [20]. We also provide a broader treatment of the full NSI parameter space by introducing all of the $\varepsilon_{\alpha\beta}$ terms into the fitting framework.

The probability formalism used in this analysis follows that shown in the MINOS+T2K combined analysis [17], where the full details of the $P(\nu_\mu \to \nu_e)$ derivation are expressed. In the limit of $\Delta m^2_{21}/\Delta m^2_{31} \to 0$, the ν_e appearance probability can be represented in terms of an effective phase, $(\delta_{CP} + \delta_{e\tau})$. In this paper, we maintain the use of this phase to simplify the presentation of the results even though we treat each CP phase separately. We also introduced computational improvements to the ν_e analysis framework that make use of fast matrix multiplication to calculate oscillation probabilities, as opposed to using channel-by-channel approximations.

The results presented here are based upon exposures of

10.6×10^{20} protons-on-target (POT) in neutrino mode and 3.3×10^{20} POT in antineutrino mode. These data were previously analyzed in the first joint ν_e+$\overline{\nu}_e$ appearance search [20].

Events in the ν_e and $\overline{\nu}_e$ charged current (CC) samples were identified using a statistical selection algorithm. Unlike the MINOS ν_μ and $\overline{\nu}_\mu$ CC analyses in which events are easily distinguished and charge-sign selected based upon the presence of muon tracks and their curvatures, ν_e analyses must address the similar topologies of the $\nu_e(\overline{\nu}_e)$ CC signal and neutral current (NC) background. A Library Event Matching (LEM) technique, adopted in previous searches [20–23], was used to compare the energy depositions of input candidates to libraries of 20 million ν_e or $\overline{\nu}_e$ CC interactions, with 30 million NC interactions in both libraries. Information gathered through this matching process was passed to an artificial neural network that returned a single-valued discriminant, $0.0 < \alpha_{LEM} < 1.0$, for each event.

Events with $\alpha_{LEM} > 0.6$, considered sensitive to ν_e and $\overline{\nu}_e$ appearance, constitute our analysis samples. The cut on α_{LEM} was established in [20] through the assessment of different binning schemes and the resulting sensitivities to θ_{13}. Assuming a three-flavor neutrino oscillation model that includes the Hamiltonian perturbation from Eq. (1), we probe the $\varepsilon_{e\tau}, (\delta_{CP} + \delta_{e\tau})$ parameter space by comparing predicted FD event counts with those observed. A simultaneous fit of the neutrino and antineutrino data is performed using a 30 bin scheme. Each configuration is represented by 15 bins with three divisions of $\alpha_{LEM} > 0.6$ and five divisions that span a reconstructed neutrino energy range of 1-8 GeV. Reconstructed energy distributions, shown in Fig. 1, compare three FD Monte Carlo predictions that illustrate standard and non-standard oscillations.

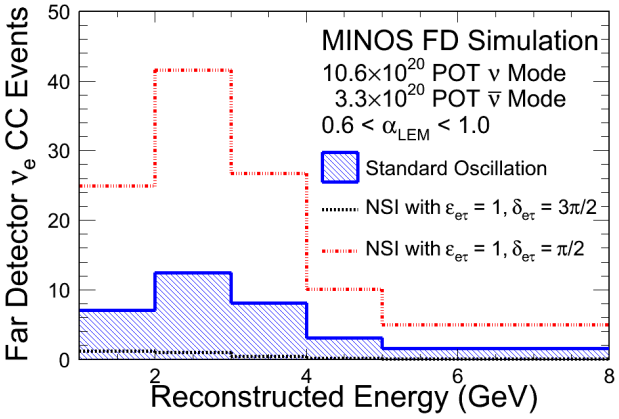

FIG. 1: Far Detector Monte Carlo ν_e CC reconstructed energy distributions shown for standard oscillation and for two illustrative non-standard oscillation cases. Normal mass hierarchy, $|\Delta m^2_{31}| = 2.41 \times 10^{-3} eV^2$, $\delta_{CP} = 0$, $\theta_{23} = \pi/4$ and $\sin^2(2\theta_{13}) = 0.084$ are assumed. Unspecified NSI parameters are set to zero.

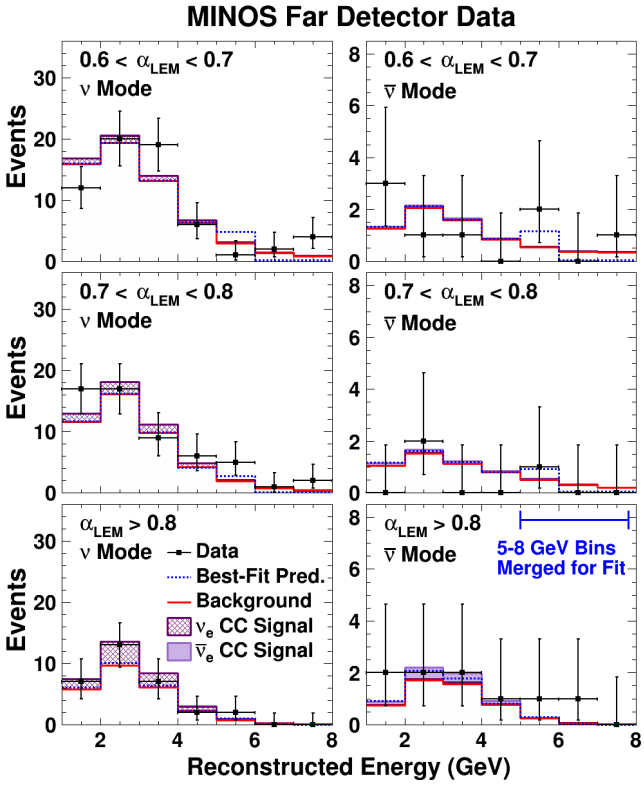

FIG. 2: The reconstructed energy distributions for three ranges of α_{LEM}. The 5-8 GeV region is combined into a single bin for the fit. The best fit that includes systematics is shown assuming normal mass hierarchy, with $\varepsilon_{e\tau} = 0.74$ and $(\delta_{CP} + \delta_{e\tau}) = 1.35\pi$. It is overlaid atop the standard oscillation predictions from [20].

Figure 2 shows the reconstructed energy distributions for data, the standard oscillation prediction, and the NSI-allowed best-fit prediction. The divisions of α_{LEM}, the splitting of neutrino and antineutrino modes, and the reconstructed energy range of the shown histograms are representative of the binning scheme used in the fit.

A two-dimensional fitting framework assessed likelihoods at values of both $\varepsilon_{e\tau}$ and $\delta_{e\tau}$ given a selected neutrino mass hierarchy and δ_{CP}. All of the produced likelihood surfaces were represented in terms of $(\delta_{CP} + \delta_{e\tau})$, and the contours for each hierarchy were generated by sampling the surfaces for different values of δ_{CP} to determine the most conservative result. Statistical and systematic uncertainties on the FD prediction were taken into account when assessing the contours. The handling of systematic errors in this analysis is identical to the prescription in [20] with one notable exception.

To account for the systematics due to the uncertainties on oscillation parameters, templates were introduced to the fitting framework that treat θ_{23}, Δm^2_{32}, and five of the NSI $\varepsilon_{\alpha\beta}$ terms as nuisance parameters. The templates were made by storing the changes in the FD prediction induced by $\pm 1\sigma$ shifts on the selected oscillation parame-

Parameter	Mean	Uncertainty
ε_{ee}	0.00	$(-4.20,+4.20)$
$\varepsilon_{e\mu}$	0.00	$(-0.33,+0.33)$
$\varepsilon_{\mu\mu}$	0.00	$(-0.07,+0.07)$
$\varepsilon_{\mu\tau}$	0.00	$(-0.01,+0.01)$
$\varepsilon_{\tau\tau}$	0.00	$(-21.0,+21.0)$
$\Delta m^2_{32}/10^{-3}$ eV^2 (NH)	+2.404	$(-0.068,+0.048)$
$\Delta m^2_{32}/10^{-3}$ eV^2 (IH)	−2.304	$(-0.058,+0.048)$
θ_{23} (NH)	0.853	$(-0.128,+0.033)$
θ_{23} (IH)	0.859	$(-0.043,+0.025)$

TABLE I: The mean values and uncertainties placed upon the nuisance parameters in the fit. Oscillation parameters with mass hierarchy dependent selections are designated with (NH) or (IH) for normal or inverted hierarchy, respectively.

Parameter	Best Fit (NH)	Best Fit (IH)
ε_{ee}	-0.26σ	-0.21σ
$\varepsilon_{e\mu}$	0.54σ	0.48σ
$\varepsilon_{\mu\mu}$	0.00σ	0.57σ
$\varepsilon_{\mu\tau}$	0.01σ	0.01σ
$\varepsilon_{\tau\tau}$	0.00σ	0.24σ
$\Delta m^2_{32}/10^{-3}$ eV^2	0.00σ	0.00σ
θ_{23}	-0.07σ	-0.08σ
$\lvert\varepsilon_{e\tau}\rvert$	0.74	0.58
$\delta_{CP}+\delta_{e\tau}$	1.35π	1.65π

TABLE II: The standard deviations from the accepted values of the oscillation parameters as determined by the fit along with the best-fit values of $|\varepsilon_{e\tau}|$ and $\delta_{CP}+\delta_{e\tau}$. Normal and inverted hierarchy are designated by (NH) and (IH) respectively.

ters in each bin of reconstructed energy and α_{LEM}. The stored predictions improved the efficiency of the fit by shortening the amount of time needed to evaluate the likelihood at each point in the parameter space. Central values and limits were taken from [24] for θ_{13}; from [25] for the other standard oscillation parameters; from [12], for $\varepsilon_{\mu\tau}$; and from [11] for the other $\varepsilon_{\alpha\beta}$ coefficients.

The mean values and uncertainties of the nuisance parameters used in the fit are included in Table I. The impact of including the nuisance parameters in the fit was investigated. Comparing the solid and dotted contours in Fig. 3, we observe that the addition of the nuisance parameters into the fit does not significantly affect the sensitivity of the analysis to the NSI parameters of interest. The standard deviations from the accepted values of these parameters, as well as the best-fit values of $\varepsilon_{e\tau}$ and $(\delta_{CP}+\delta_{e\tau})$, are provided in Table II.

The shaded regions in Fig. 3 show the allowed ranges of $\varepsilon_{e\tau}$ given an effective CP phase and choice of neutrino mass hierarchy. In both cases, the allowed region is consistent with predictions of the standard oscillation model. These results yield modest improvement over the model-independent limit established in [26], which set $|\varepsilon_{e\tau}| < 3.0$ for propagation through Earth-like material, and the limits are consistent with the MINOS+T2K result presented in [17].

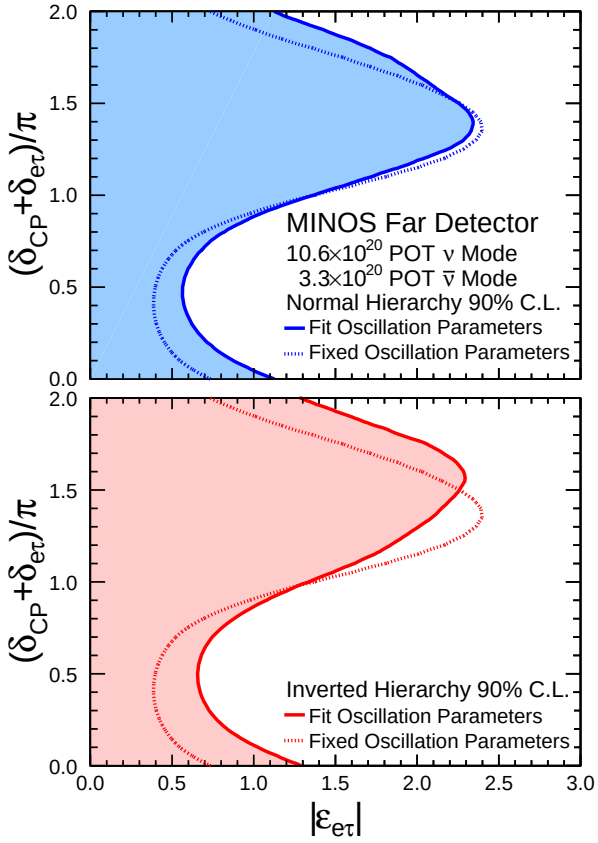

FIG. 3: 90% C.L. in the $\varepsilon_{e\tau}, (\delta_{CP}+\delta_{e\tau})$ parameter space for normal (top) and inverted (bottom) neutrino mass hierarchy using ν_e and $\overline{\nu}_e$ appearance candidates in the MINOS Far Detector. The shaded areas to the left of the solid contours indicate the MINOS allowed regions where additional oscillation parameters, including NSI, were included in the fit. The dotted contours show the limits where the additional oscillation parameters were fixed to the mean values shown in Table I.

In summary, we have performed a direct search for non-standard interactions using the full sample of ν_e and $\overline{\nu}_e$ appearance candidates in the MINOS FD. Using a statistical selection algorithm to identify ν_e and $\overline{\nu}_e$ events, we performed a simultaneous, two-dimensional fit to neutrino and antineutrino samples to place limits upon the $\varepsilon_{e\tau}, (\delta_{CP}+\delta_{e\tau})$ parameter space. We found no evidence for non-standard neutrino interactions. The results provide improvement on existing constraints from independent models and are comparable to the previous limit established using MINOS and T2K data.

This work was supported by the U.S. DOE; the United Kingdom STFC; the U.S. NSF; the State and University of Minnesota; and Brazil's FAPESP, CNPq and CAPES. We are grateful to the Minnesota Department of Natural Resources, the crew of the Soudan Underground Lab, and the personnel of Fermilab for their contribution to this effort. We thank the Texas Advanced Computing Center

at The University of Texas at Austin for the provision of computing resources.

* Now at Lancaster University, Lancaster, LA1 4YB, UK.
† Now at South Dakota School of Mines and Technology, Rapid City, South Dakota 57701, USA.
‡ Deceased.

[1] Y. Ashie *et al.* (Super-Kamiokande), Phys. Rev. Lett. **93**, 101801 (2004); Phys. Rev. D **71**, 112005 (2005).
[2] B. Aharmim *et al.* (SNO), Phys. Rev. C **72**, 055502 (2005).
[3] D. G. Michael *et al.* (MINOS), Phys. Rev. Lett. **97**, 191801 (2006); P. Adamson *et al.* (MINOS), Phys. Rev. D **77**, 072002 (2008).
[4] T. Araki *et al.* (KamLAND), Phys. Rev. Lett. **94**, 081801 (2005).
[5] C. Arpesella *et al.* (Borexino), Phys. Rev. Lett. **101**, 091302 (2008).
[6] M. H. Ahn *et al.* (K2K), Phys. Rev. D **74**, 072003 (2006).
[7] F. P. An *et al.* (Daya Bay), Phys. Rev. Lett. **108**, 171803 (2012); J. K. Ahn *et al.* (RENO), Phys. Rev. Lett. **108**, 191802 (2012).
[8] B. Pontecorvo, JETP **7**, 172 (1958); V. N. Gribov and B. Pontecorvo, Phys. Lett. B **28**, 493 (1969); Z. Maki, M. Nakagawa, and S. Sakata, Prog. Theor. Phys. **28**, 870 (1962).
[9] L. Wolfenstein, Phys. Rev. D **17**, 2369 (1978); S. P. Mikheyev and A.Yu. Smirnov, Sov. J. Nucl. Phys. **42**, 913 (1985); J. W. F. Valle, Phys. Lett. B **199**, 432 (1987).
[10] M. C. Gonzalez-Garcia *et al.*, Phys. Rev. Lett. **82**, 3202 (1999); A. Friedland, C. Lunardini, and M. Maltoni, Phys. Rev. D **70**, 111301 (2004).
[11] T. Ohlsson, Rep. Prog. Phys. **76**, 044201 (2013).
[12] G. Mitsuka *et al.* (Super-Kamiokande), Phys. Rev. D **84**, 113008 (2011).
[13] P. Adamson *et al.* (MINOS), Phys. Rev. D **88**, 072011 (2013).
[14] W. A. Mann *et al.*, Phys. Rev. D **82**, 113010 (2010).
[15] J. Kopp, P. A. N. Machado, S. J. Parke, Phys. Rev. D **82**, 113002 (2010).
[16] Z. Isvan, FERMILAB-THESIS-2012-03, University of Pittsburgh, (2012).
[17] J. A. B. Coelho *et al.*, Phys. Rev. D **86**, 113015 (2012).
[18] D. G. Michael *et al.*, Nucl. Instrum. and Meth. A **596**, 190 (2008).
[19] P. Adamson *et al.* (MINOS), Nucl. Instr. and Meth. A **806**, 279 (2016).
[20] P. Adamson *et al.* (MINOS), Phys. Rev. Lett. **110**, 171801 (2013).
[21] R. Toner, FERMILAB-THESIS-2011-53, University of Cambridge, (2011).
[22] A. P. Schreckenberger, FERMILAB-THESIS-2013-04, University of Minnesota, (2013).
[23] P. Adamson *et al.* (MINOS), Phys. Rev. Lett. **107**, 181802 (2011).
[24] F. P. Ahn *et al.* (Daya Bay), Phys. Rev. Lett. **115**, 111802 (2015).
[25] D. V. Forero, M. Tórtola, and J. W. F. Valle, Phys. Rev. D **90**, 093006 (2014).
[26] C. Biggio, M. Blennow, and E. Fernández-Martínez, JHEP **08**, 090 (2009).